Journal of Volcanology and Geothermal Research 448 (2024) 108017

Contents lists available at ScienceDirect

Journal of Volcanology and Geothermal Research

journal homepage: www.journals.elsevier.com/journal-of-volcanology-and-geothermal-research

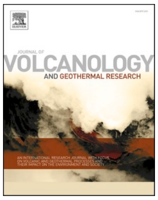

Submarine pyroclastic deposits from 7.3 ka caldera-forming Kikai-Akahoya eruption

Satoshi Shimizu [a,b,*], Reina Nakaoka [a,c], Nobukazu Seama [c,a], Keiko Suzuki-Kamata [a], Katsuya Kaneko [c,a], Koji Kiyosugi [a,c], Hikaru Iwamaru [a,d], Mamoru Sano [a,d], Tetsuo Matsuno [a], Hiroko Sugioka [a,c], Yoshiyuki Tatsumi [a]

[a] *Kobe Ocean-Bottom Exploration Center, Kobe University, Kobe, Japan*
[b] *Seisgadget Ltd., Tokyo, Japan*
[c] *Department of Planetology, Graduate School of Science, Kobe University, Kobe, Japan*
[d] *Nippon Marine Enterprises, Ltd., Yokosuka, Japan*

ARTICLE INFO

Keywords:
Kikai caldera
Pyroclastic density current
Submarine
Seismic reflection

ABSTRACT

Extensive submarine pyroclastic deposits were discovered around the Kikai caldera, Southwest Japan, which originated from the caldera-forming Kikai-Akahoya (K-Ah) eruption that occurred at 7.3 ka. This submarine pyroclastic unit originated from a pyroclastic density current (PDC) that entered the sea and was transformed into a subaqueous density current. Our high-resolution marine seismic reflection surveys reveal that the uppermost unit exhibiting prominent seismic facies thins radially away from the caldera and covers >4500 km^2 of the seafloor. The estimated volume of the submarine deposits is >71 km^3 based on the isopach map. Seismic sequence stratigraphic analyses and correlation of shard glass compositions from the piston core and remotely operated vehicle samples with those from subaerial outcrops identified the unit as pyroclastic deposits produced by the K-Ah eruption. The geomorphological features of the unit indicate a long runout distance (i.e., 40 km), exponential thinning with increasing distance from the source, and a depression-filling nature of the deposits suggesting that the unit was formed predominantly by a density current that entered the water. The quantitative comparisons of geometric shape and its thinning rate, including that for non-volcanic density currents, indicate that the subaerial PDC entering into the water was transported as a dilute density current in the water. We propose that the formation of these dilute density currents transformed by PDCs probably requires sufficient water depth, as inferred also from previous analog experiments. Adding on-land ignimbrite of 5 km^3 and widespread tephra of 249–374 km^3, our estimate of submarine pyroclastic deposits of >71 km^3 leads to a total bulk volume of the K-Ah eruption of 332–457 km^3 (133–183 km^3 in DRE), making it probably the largest eruption of the Holocene.

1. Introduction

Caldera-forming explosive eruptions eject felsic magma as voluminous pyroclastic density currents (PDCs) and ashfall over broad areas. PDCs are produced from the collapse of explosive eruption columns and propagate over long distances. Many caldera-forming eruptions occur on oceanic islands and continental margins at subaerial or shallow-water vents; once PDCs reach the water, some parts of the pyroclastic material enter into the water and other parts travel across it. Ultimately, a substantial portion of the pyroclastic products becomes deposited on the seafloor. PDCs traveling over water are known from the Kos Plateau Tuff, Greece (Allen and Cas, 2001), the Campania ignimbrite, Naples (Fisher et al., 1993), the 1883 eruption of Krakatau (Carey et al., 1996) and Koya ignimbrite of Kikai (Ui, 1973; Walker et al., 1984; Maeno and Taniguchi, 2007), and have been observed at the modern volcano of Soufriere Hills, Montserrat (Cole et al., 1998). The Koya ignimbrite is the PDC deposit derived from the 7.3 ka Kikai-Akahoya (K-Ah) caldera-forming eruption, and it was deposited on distal islands after being

---

Abbreviations: DRE, dense rock equivalent; JAMSTEC, Japan Agency for Marine-Earth Science and Technology; K-Ah, Kikai-Akahoya; PDC, pyroclastic density current; ROV, remotely operated vehicle.

[*] Corresponding author at: Kobe Ocean-Bottom Exploration Center, Kobe University, Kobe, Japan.

E-mail address: shimizu@harbor.kobe-u.ac.jp (S. Shimizu).

https://doi.org/10.1016/j.jvolgeores.2024.108017
Received 12 August 2023; Received in revised form 20 January 2024; Accepted 29 January 2024
Available online 1 February 2024
0377-0273/© 2024 The Authors. Published by Elsevier B.V. This is an open access article under the CC BY license (http://creativecommons.org/licenses/by/4.0/).

transported over the sea (Ui, 1973; Walker et al., 1984; Maeno and Taniguchi, 2007).

The transport and emplacement mechanisms of PDCs entering water remain a subject of discussion that has been written about extensively (Sparks and Huang, 1980; Mandeville et al., 1996; Mcleod et al., 1999; Freundt, 2003; Trofimovs et al., 2008; Allen et al., 2012; Jutzeler et al., 2017; Freundt et al., 2022). Cas and Wright (1991) discussed the interaction between PDCs and water, and their modern and ancient subaqueous deposits, based on an evaluation of known documented case studies. They pointed out that in most cases, the interaction of PDCs with water results in two main processes 1) the loss of heat and interstitial gas contained by the subaerial PDCs followed by entrainment of water and 2) the conversion to water-supported density currents. Some of the pyroclastic material advancing over water, accelerated by phreatic explosions when the flow is hot and detaches from the main flow and mixes with water, causing sinking sediment plumes that merge with the water-supported density current (Freundt, 2003; Freundt et al., 2022).

The thickness and runout distance of PDCs are fundamental properties that represent their underlying dynamics (Bursik and Woods, 1996; Dade and Huppert, 1996; Cas et al., 2011; Roche et al., 2016). Many PDC deposits on-land exhibit gradual thinning with increased distance from the source in an exponential fashion (Wilson, 1991; Silleni et al., 2020). However, no definitive geological evidence exists regarding the exponential thinning of submarine deposits. The reasons for this may be due to the lack of field data, the water depth environment, and secondary mass movements (turbidites, debris flows, and avalanches) that are not observable. The distribution and volume of the pyroclastic material deposited on the modern seafloor around the source have been studied at a few volcanoes such as the Minoan eruption of Santorini (Sigurdsson et al., 2006; Karstens et al., 2023), the Roseau Tuff of Dominica (Carey and Sigurdsson, 1980) the Soufrière Hills of Montserrat (Hart et al., 2004; Trofimovs et al., 2008, 2012; Karstens et al., 2013), and the 1883 eruption of Krakatau (Sigurdsson et al., 1991; Self, 1992; Mandeville et al., 1996). Subaerial PDCs, originating from the 2003 dome collapse during a small-scale eruption of the Soufrière Hills Volcano in the Lesser Antilles, were witnessed and investigated. A large portion of these subaerial PDCs became deposited in the submarine environment; and were characterized as water-supported density currents (e.g., Trofimovs et al., 2008). Meanwhile, the 1883 Krakatau eruption is a well-documented example of subaqueous deposition proximal to the source with an average water depth of 40 m; these marine deposits do not exhibit systematic thinning with increasing distance from the source (Mandeville et al., 1996).

The transport and sedimentation processes of pyroclastic material entering water have also been studied with laboratory experiments and theoretical modeling (McLeod et al., 1999; Legros and Druitt, 2000; Freundt, 2003; Freundt et al., 2022; Allen et al., 2012). Freundt (2003) conducted laboratory experiments and the results indicated that the seafloor-hugging density current deposits exhibit exponential thinning with increasing distance from the source. In these experiments, ash introduced into a water-filled tank created different flow conditions. Subaerial flow caused steam explosions and flowed over the water surface, while the subaqueous flow mixed with water, forming ash plumes and seafloor-hugging density currents that thinned out exponentially with distance. This study highlighted the importance of water depth in determining the transport and deposition of particles. That is, seafloor-hugging density currents are formed in deep-water settings, while they do not occur in shallow-water settings at least in the area proximal to the source. Further, they showed that a smooth transition of the bulk flow from air into water does not occur until the flow thickness is >40–60% of the water depth. Thus, it is necessary to investigate the distribution of pyroclastic deposits originating from a modern large eruption in sufficiently deep water to better understand the dynamics of the PDC-water interaction.

In this study, we present evidence of deposits produced by a water-supported density current transformed from the PDC generated by the 7.3 ka caldera-forming Kikai-Akahoya (K-Ah) eruption. We present the results of high-resolution marine seismic reflection surveys covering a large area around the submarine Kikai caldera and chemical analyses of volcanic glasses sampled by piston coring and a remotely operated vehicle (ROV). Considering that the submarine deposits have been well preserved in the deep-sea environment without prominent erosions or overburdens over the past 7300 years, we also identified submarine deposits that provide a precise spatial extent and improved the volume estimate of the K-Ah eruption. These deposits are the submarine counterpart of the subaerial PDC deposits (the Koya ignimbrite), which were emplaced after traveling over the sea around the caldera. Based on the exponential thinning and depression-filling nature of the submarine deposits, we discuss the behavior of pyroclastic material after its transformation into water-supported density currents. In addition, we compare the behavior of non-volcanic density currents that form long runout turbidities. Finally, we propose an emplacement mechanism involving the water-supported density current transformed from the subaerial PDC, as the predominate origin.

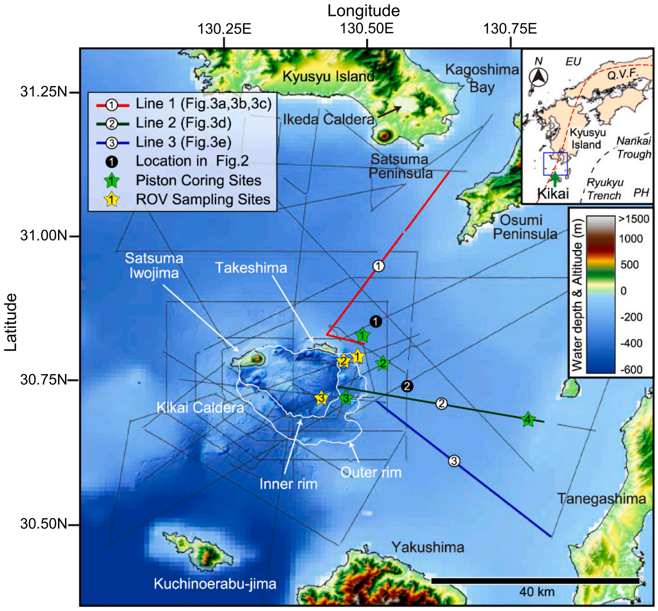

Fig. 1. Location of the Kikai caldera, south of Kyusyu Island, SW Japan, situated on the Quaternary volcanic front of the SW Japan arc.
Inner and outer caldera rims of the Kikai caldera are shown by white solid lines (Tastumi et al., 2018). Seismic lines are shown in black, and some of them are thick colored and numbered to indicate the seismic sections in the following figures (All the seismic sections are shown in the supplementary figures). Locations of pyroclastic samples obtained by piston coring (PC-1 to PC-4) and ROV (KC-1 to KC-3) are indicated by green and yellow stars, respectively. Bathymetry around the Kikai caldera was obtained by our survey; the other bathymetry and on-land topography are drawn by using 500-m mesh J-EGG and EarthEnv-DEM90 (Robinson et al., 2014), respectively. EU, Eurasia plate; PH, Philippine Sea plate; Q.V.F., Quaternary volcanic front. (For interpretation of the references to colour in this figure legend, the reader is referred to the web version of this article.)

2. Kikai caldera

The Kikai caldera is located south of Kyusyu Island in SW Japan. It sits across the volcanic front (Fig. 1) where the Philippine Sea plate subducts the Eurasian plate. The caldera has produced at least three large-scale eruptions, i.e., 140, 95, and 7.3 ka (Ono et al., 1982; Machida and Arai, 2003). The latest eruption, known as the K-Ah eruption, is one of the most voluminous Holocene eruptions and was accompanied by a submarine caldera collapse. The Kikai caldera is composed of an outer and an inner caldera with major and minor axes of 24 and 19 km, and 17

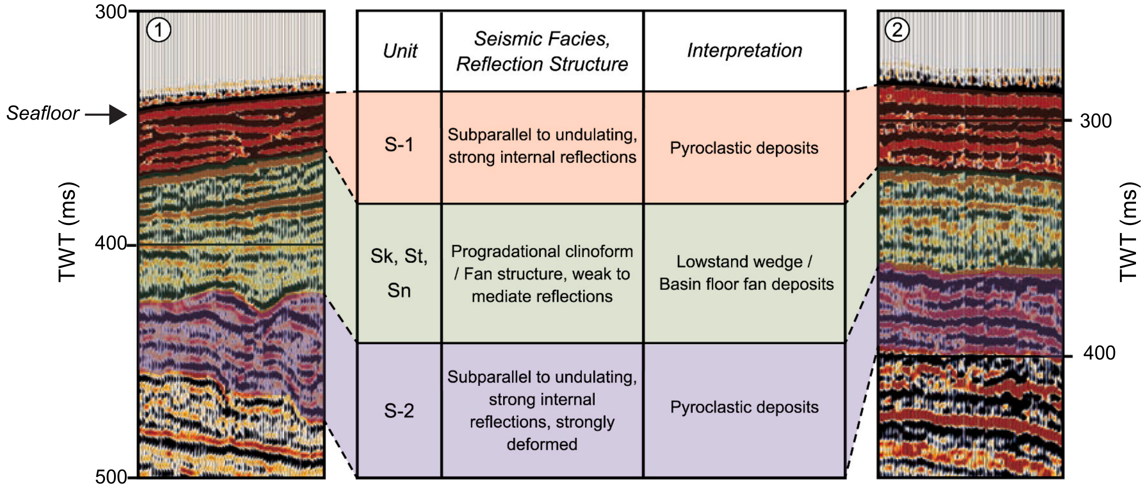

Unit	Seismic Facies, Reflection Structure	Interpretation
S-1	Subparallel to undulating, strong internal reflections	Pyroclastic deposits
Sk, St, Sn	Progradational clinoform / Fan structure, weak to mediate reflections	Lowstand wedge / Basin floor fan deposits
S-2	Subparallel to undulating, strong internal reflections, strongly deformed	Pyroclastic deposits

Fig. 2. Typical seismic facies and structures around the Kikai caldera.
Locations of each section are shown in Fig. 1. Units S-1 and S-2 are distributed around the Kikai caldera; their thicknesses decrease with increasing distance from the caldera. Units Sk, Sn, and St are depositional systems supplied from the Kyusyu, Tanegashima, and Takeshima Islands, respectively.

and 15 km, respectively (Tatsumi et al., 2018). The caldera was formed in a basin with a water depth of approximately 200 m, surrounded by the Kyusyu, Tanegashima, Yakushima, and Kuchinoerabu-jima Islands. The inner caldera has a maximum depth of approximately 600 m, including >400 m of vertical displacement from the seafloor around the caldera, and holds a giant submarine lava dome that developed after the 7.3 ka eruption (Tatsumi et al., 2018). The Satsuma Iwojima and Takeshima Islands are parts of the caldera rim exposed on the northern and western area of the caldera rim, while the southwest area deepens toward the Okinawa Trough.

The 7.3 ka K-Ah eruption commenced with a Plinian pumice fall and intraplinian PDCs, followed by a climactic phase involving voluminous PDC—known as the Koya ignimbrite over the sea, which can be traced over Kyushu Island up to 80 km distance from the source caldera. The widespread tephra layer dispersed by co-ignimbrite ash fall, known as Akahoya ash, blanketed >2,800,000 km^2 of the Japanese Archipelago (Machida, 1999; Suto et al., 2007). The climactic PDCs emplaced a < 30 m subaerial unit in the proximal Satsuma Iwojima and Takeshima Islands. This unit is subdivided into three subunits, C1, C2, and C3. Units C1 and C2 are observed only in topographic lows in Satsuma Iwojima Island. The only C3 was emplaced as a thin (i.e., < 2 m) unit corresponding to the low-aspect-ratio Koya ignimbrite in the distal islands of Kyusyu, Tanegashima, Yakushima, and Kuchinoerabu-jima (Ui, 1973; Walker et al., 1984; Maeno and Taniguchi, 2007). The volumes of the Plinian fallout, PDC, and co-ignimbrite ashfall deposits are 7, 30–45, and 374 km^3, respectively (Suto et al., 2007; Maeno and Taniguchi, 2007). The 7.3 ka K-Ah eruption is thought to have occurred near sea level based on the lithological study of the subaerial ignimbrite (Maeno and Taniguchi, 2007). While the subaerial unit in the distal islands indicates that a part of the climactic PDC encountered the surrounding water traveled over the sea (Ui, 1973; Walker et al., 1984; Maeno and Taniguchi, 2007), it should be noted that little is known about the existence and nature of these submarine deposits.

3. Material and methods

Seismic reflection surveys were conducted between 2016 and 2019 by T/S Fukae Maru of Kobe University. The seismic system was optimized for high-resolution seismic imaging, involving a mini-GI gun configured by a 30 cubic inch generator and a 30 cubic inch injector, and a hydrophone streamer composed of 6-channel hydrophones with a 6.25 m group interval. To obtain a high-frequency seismic bandwidth, the gun and streamer were towed at 3 and 2 m depth below the sea surface, respectively. The gun was fired every 8 s with a 4.5-knot average towing speed. The reflection signals were recorded at 1-msec sampling intervals. Seismic data processing involved the following steps: field file editing, static correction, band-pass filter, amplitude recovery, constant velocity stack with a 12.5 m bin, and Stolt migration. The overall seismic data maintained a wide frequency range of 50–260 Hz, with a 150 Hz dominant frequency. This configuration provided ~2 m vertical resolution (i.e., a quarter of the dominant wavelength) for stratigraphic interpretation of the depositional successions and revealed detailed features of the targeted units with a reasonable penetration depth of several hundred meters below the seafloor.

Seabed sampling was performed using a piston corer and an ROV. Piston coring with various core barrels (i.e., 6–8 m) was operated by R/V Shinsei Maru of the Japan Agency for Marine-Earth Science and Technology (JAMSTEC) in 2019. The ROV was operated by T/S Fukae Maru in 2018 and seafloor sediments were collected using a suction sampler. The major elements in the volcanic glasses obtained from both samples were analyzed using an electron-probe microanalyzer (JEOL-8900 EPMA) at Kobe University. The analysis parameters were 15 kV accelerating voltage, 12 nA beam current, and 10 μm defocused electron beam.

4. Results

4.1. Seismic facies and distribution

Comprehensive stratigraphic analyses of seismic reflection data along 75 lines covering a wide area around the Kikai caldera off Kyusyu Island (Fig. 1) enabled the subdivision of the top ~100 m subsurface strata into five characteristic units (Fig. 2). Units S-1 and S-2 are extensively distributed around the Kikai caldera and tend to thin radially with increasing distance from the caldera, indicating that they are deposits derived from this area. Units Sk, Sn, and St form system tracts likely to be sedimentary successions supplied from the Kyusyu, Tanegashima, and Takeshima Islands, respectively.

Unit S-1 is the uppermost unit spread over the entire surveyed area, exhibiting seismic facies characterized by high-amplitude, semi-continuous, and subparallel internal reflectors with irregular wavelengths of tens to hundreds of meters (Fig. 3). Additionally, this unit exhibits seismically transparent facies only near the Satsuma Iwojima Island, and a gradual transition to typical facies with subparallel and undulating structures. The thickness of unit S-1 tends to decrease with increasing distance from the caldera, i.e., > 20 m around the caldera

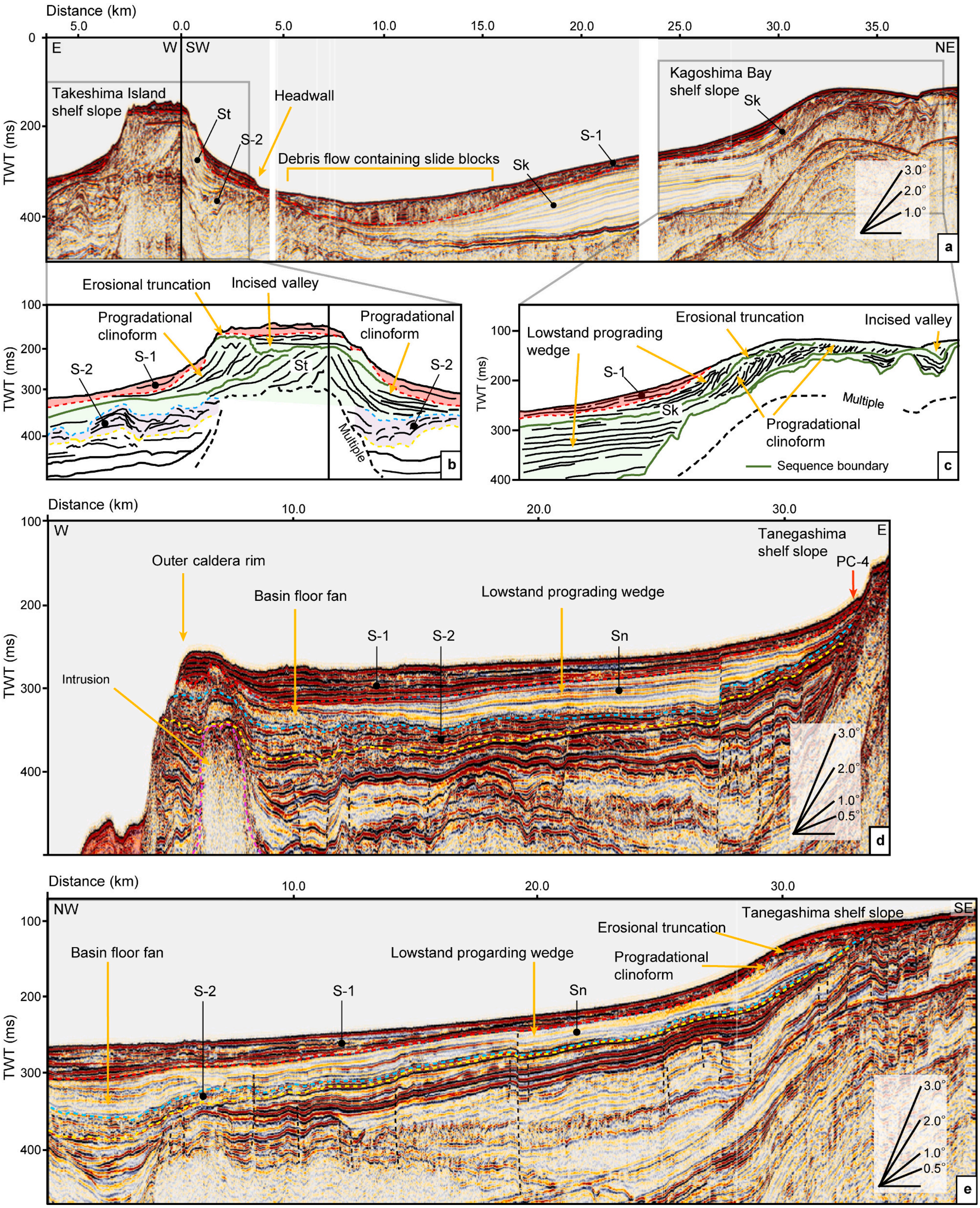

Fig. 3. Interpretation of seismic sections.
(a) Seismic section line 1 extends from the north of the Takeshima Island (SW) to the mouth of the Kagoshima Bay (NE). Unit S-1, delineated by a red dashed line along its lower boundary, covers a broad extent of seafloor from SW to NE. Units Sk and St represent the depositional systems supplied from the Kagoshima Bay and Takeshima Island, respectively. Unit S-2 is represented by a right blue dashed line and a yellow dashed line for its upper and lower boundary. (b–c) Seismic interpretations of the depositional systems on both ends of line 1. Units Sk and St consist of system tracts developed from the mid-shelf to the basin. An erosional truncation is recognized as a top lap surface of progradational clinoforms in units Sk and St. (d–e) Seismic section lines 2 and 3 located on the east side of the caldera. Unit S-1 extends from the eastern caldera rim to the western slope of Tanegashima Island. Unit S-1 is cut by the outer caldera rim on the west of (d) and thinning toward the shelf. Unit S-1 fills pre-existing topographic lows under the unit S-1. Piston-cored point PC-4 is located at the eastern end of unit S-1 on (d). (For interpretation of the references to colour in this figure legend, the reader is referred to the web version of this article.)

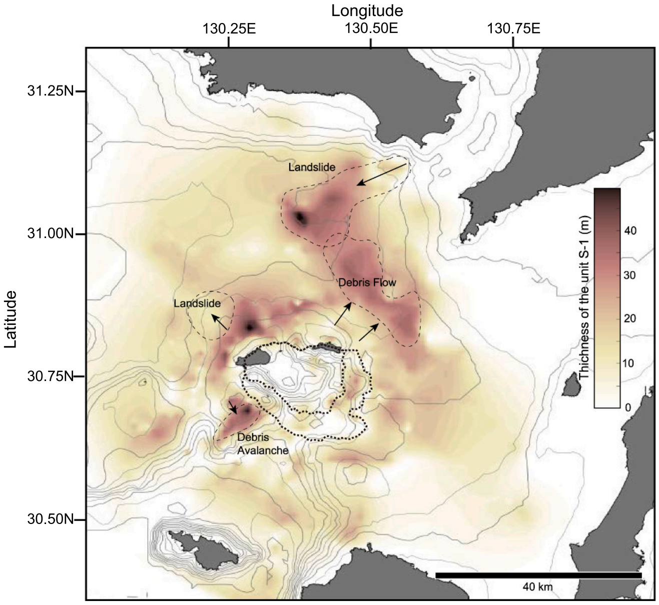

Fig. 4. Isopach map of unit S-1 calculated from the integrated seismic interpretation.
Inner and outer caldera rims are shown by thickening the lines (Tatsumi et al., 2018). The center of the caldera is filled by the caldera dome.

rim, particularly >30 m in the north to west of the caldera rim around the Satsuma Iwojima Island and ~ 3 m at ~40 km distance. There is also a thick accumulated region at the center of the basin between the Kyusyu Island and Kikai caldera that exhibits chaotic facies and contains blocks retaining high-amplitude subparallel facies (Fig. 3a). Unit S-1 was often cut or terminated abruptly by the outer caldera wall (Fig. 3d). The characteristic feature of unit S-1 is that it blankets the seafloor and fills basins, depressions, and fault-related displacements to form a rather smooth submarine topography (Fig. 3d and e).

Unit S-2, with a 30 m maximum thickness, is also characterized by a high-amplitude, semi-continuous, subparallel, and undulating structure, similar to the facies of unit S-1, and is often deformed by faulting and slumping, particularly around Takeshima Island, to form large sliding blocks (Fig. 3b). We stress that the thickness of this unit, similar to that of unit S-1, decreases concentrically with increasing distance from the Kikai caldera along the basin to the slope of Kyusyu and Tanegashima Islands (Fig. 3a, d, and e), suggesting that both units may be composed of caldera-derived pyroclastic deposits.

Units Sk, Sn, and St form system tracts likely composed of detrital sediments supplied from the Kyusyu, Tanegashima, and Takeshima Islands, respectively, and are well stratified, having weak- to moderate-amplitude units, while large portions are covered by unit S-1. These units form a fan-shaped distribution on the slope to the basin floor from the Kyusyu, Tanegashima, and Takeshima Islands, represent packages of successive systems tracts supplied from those islands (Fig. 3), and can be subdivided into depositional sequences and systems tracts. Sigmoid-oblique progradational clinoforms are commonly formed on the shelf edges of Kagoshima Bay, and the Tanegashima and Takeshima Islands, with erosional truncation on their top lap surfaces (Fig. 3). Parallel reflections over chaotic incised valley-fill deposits were evident on the mid-shelf of Kagoshima Bay and the Takeshima Island.

The results from the high-resolution seismic reflection surveys allowed us to edit the isopach map for unit S-1 (Fig. 4) based on the following three assumptions. First, the thickness of unit S-1 along each seismic line was converted from the two-way travel time with 1500 m/s sound velocity, corresponding to the minimum velocity and providing a minimum thickness estimate. Second, we ignored layers thinner than ~3 m, since this was the resolution limit for discriminating the facies in the present seismic bandwidth. Third, in the area between the seismic lines, the layer thickness was linearly interpolated. The distributed area of unit S-1 was then estimated to be >4500 km^2.

4.2. Composition of glass shards in unit S-1

The origin of unit S-1 was examined by comparing the compositions of pyroclasts from unit S-1 with both those of the K-Ah and post-K-Ah deposits. We reconfirmed the chemical characteristics of the K-Ah and post-K-Ah ejecta, as well as the compositional differences between them. Juvenile pumices, scoria and volcanic ash were separated from the Koya ignimbrite on Takeshima Island, which is located on the caldera rim (Fig. 1). The analyzed post-K-Ah volcanics were rhyolite from the submarine giant lava dome (Tatsumi et al., 2018), lava flows from the Showa Iwojima Island, pumice flows from the Iwo-dake Volcano, and scoria falls from the Inamura-dake Volcano on the Satsuma Iwojima Island (Saito et al., 2001). The groundmass compositions of juvenile fragments and lava samples, as well as those of glass shards from volcanic ash samples, were determined using an electron-probe microanalyzer. Chemical analyses provided the compositional difference between the K-Ah and post-K-Ah ejecta (Fig. 5). Both magmas exhibited bimodal compositions, however, a dacitic magma (i.e., 65–70 wt% SiO_2) was erupted solely in the K-Ah eruption, while post-K-Ah magmas (i.e., ~58 and 77–78 wt% SiO_2) had lower or slightly higher SiO_2 concentration than K-Ah magmas (i.e., ~65 and 74–75 wt% SiO_2).

The chemical characteristics of the volcanic glasses from the piston-cored and ROV samples showed that unit S-1 is the submarine equivalent to the Koya ignimbrite. Samples of unit S-1 were directly collected by piston coring at four sites, where the seismic reflection results suggested that the unit was distributed at the uppermost seabed (Fig. 1). Piston coring recovered samples with lengths of 2, 2, 1, and 6 m at sites PC-1, PC-2, PC-3, and PC-4, respectively. Samples for our chemical analyses were taken from the lower part of the core to avoid possible surface deposits containing products of small-scale post-caldera activity: The sampling depth is retained in the core because the core is not disturbed even though the core was slightly poorly recovered and contained water, making it difficult to identify the depositional structure. The samples likely consisted primarily of unit S-1, as they are composed of juvenile pumices and finer ashes, which are consistent with subaerial Koya ignimbrite. Samples from the PC-1, PC-2, and PC-3 sites in the proximal area contained cm-sized pumice (i.e., several centimeters), whereas those from the PC-4 site in the distal area contained mm-sized pumice (i.e., several millimeters). The volcanic glasses separated from the PC-1 and PC-2 samples exhibited a bimodal compositional distribution with major and minor peaks at 74 and 65 wt% SiO_2, respectively. These compositions are identical to those of subaerial ignimbrites in the K-Ah eruption. The PC-3 and PC-4 samples did not exhibit a clear compositional peak at ~65 wt% SiO_2. However, the peak at 74 wt% SiO_2 was identical to those of PC-1, PC-2, and Koya ignimbrites while being distinct from those of post-K-Ah volcanics. PC-3 and PC-4 samples may represent the early-stage of the ignimbrite unit proposed in previous studies (i.e., Fujihara and Suzuki-Kamata, 2013; Geshi et al., 2017) documented that the amount of glass shards with low SiO_2 content varies even within a subaerial single ignimbrite unit. In these samples, minimal amounts of low SiO_2 glass shards were found in the lower region, which erupted during the early-stage of the eruption, and increased upwards as the eruption progressed. Volcanic ash samples were collected by the ROV from seafloor sediments at three sites, where unit S-1 was distributed within or near the caldera wall (Fig. 1). Samples were taken while monitoring the seabed covered by pyroclastics using a video camera. Although pyroclastics consist primarily of pumice, volcanic rock, and volcanic ash, shells, and other debris may also be present on seabed. Volcanic glass shards recovered by ROV sampling revealed a wide range of SiO_2 content and a compositional peak at 75–77 wt%. Nevertheless, retrieving pyroclastics with 65–70 wt% SiO_2 is an important finding showing that volcanic glasses with 75 and 65 wt%

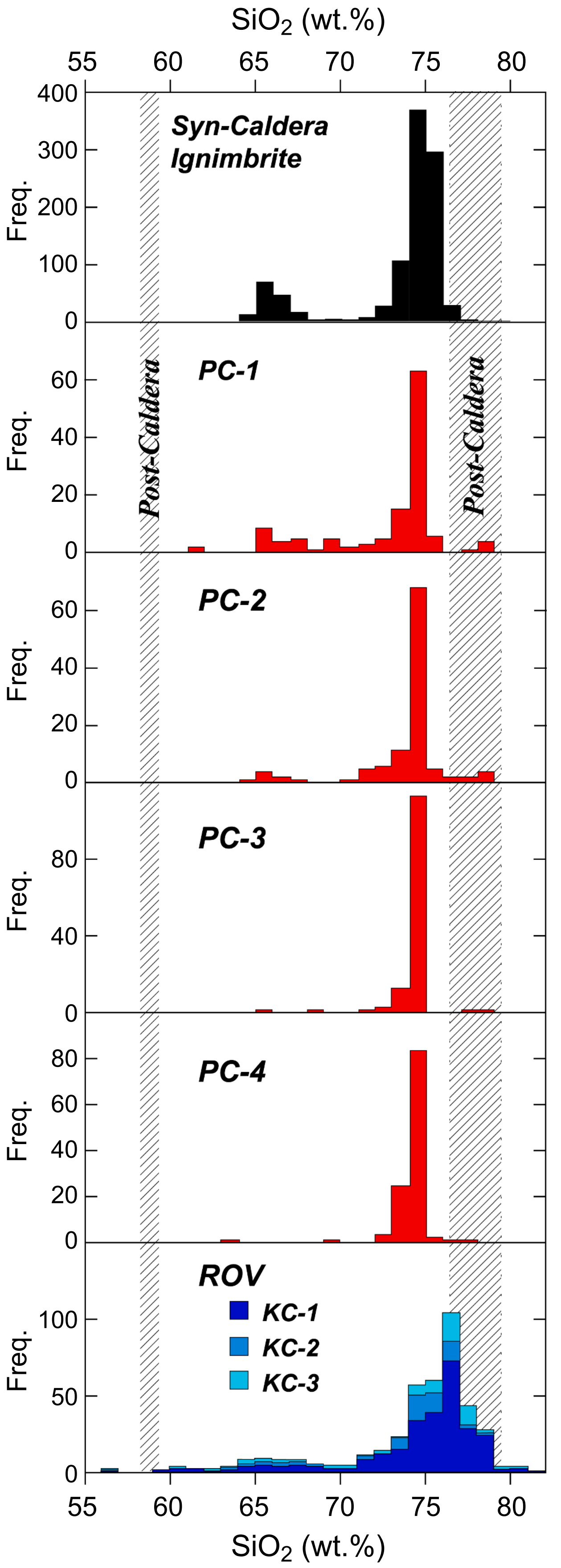

(caption on next column)

Fig. 5. Frequency distribution of SiO_2 contents in glass shards of the Kikai-Akahoya products, piston-cored samples from PC-1 to PC-4, and ROV samples from KC-1 to KC-3.

Syn-caldera ignimbrite was obtained from Koya ignimbrite at Takeshima Island located on the caldera rim. The SiO_2 ranges of the post-caldera products (hatched area) include a submarine giant lava dome (Tatsumi et al., 2018), lava on the Showa Iwojima Island, and scoria and pumice on the Satsuma Iwojima Island (Saito et al., 2001). SiO_2 values are recalculated for the total weight to 100 wt%.

SiO_2 from the K-Ah eruption does exist while also revealing a wider range of SiO_2 contents, suggesting possible surface veneer deposits containing products of small-scale post-caldera activities. This feature contrasts all the piston-cored samples obtained from far away locations (i.e., PC-4, which has a prominent peak at 75 wt% indicating no post-K-Ah compositions). Collectively, these results indicate that unit S-1 is composed of K-Ah eruption components and that post-K-Ah products are thinly deposited on the surface within the vicinity of the caldera.

5. Discussion

5.1. Age of unit S-1

Our stratigraphic interpretation corroborated that unit S-1 was emplaced during the K-Ah eruption. The distinct seismic facies of units Sk, Sn, and St around the Kikai caldera that underlie unit S-1 strongly constrain the formation age of unit S-1 (Fig. 3). Erosional structures on their toplap surfaces of the progradational clinoforms developed at the shelf edge and lowstand wedges at the seaward of the shelf break. The level of this erosion surface is 120–130 m below the current sea-level (Fig. 3) and close to that during the last glacial period, i.e., ~18 ka (Saito, 1998). These distinct erosional structures and progradational clinoforms are key identifiers of low sea-level deposition, particularly shallow-marine, near-surface depositions during the late Quaternary rapid eustatic change (e.g., Suter et al., 1987). Such depositional systems have been reported worldwide. An example close to this area is a sequence in the shelf margin of the Korea Strait, East China Sea, with depositional ages of 15–50 ka (Yoo and Park, 1997). This strait was connected to Kyushu Island during the low sea-level period of the last glacial maximum (Park et al., 1996). These lowstand wedges developed before and after the last glacial period, i.e., ~18 ka; hence, unit S-1, which overlies these structures, was therefore deposited after this period.

The reported 7.3 ka K-Ah eruption of Kikai caldera is younger than the last glacial maximum of ~18 ka and coincides with the stratigraphic position of unit S-1. The most voluminous event after the K-Ah eruption was likely the formation of a giant (i.e., $> 32\ km^3$) lava dome, which may have emerged through inflation of an endogenous lava dome, and its surface was covered by lava flows as exogenous growth (Tatsumi et al., 2018). This large, yet rather not explosive, eruption occurred solely within the inner caldera wall and provided little evidence for supplying pyroclastics to the region outside of the caldera. Other post-caldera activities at the Iwo-dake and Inamura-dake volcanoes, and the Showa Iwojima Island are all less-voluminous with a dense rock equivalent (DRE) volume of 1.10, 0.10, and 0.01 km^3, respectively (Yamamoto, 2015). Volcanism besides that of the Kikai caldera is also limited: The Ikeda caldera located in the Satsuma Peninsula (Fig. 1) produced pyroclastic deposits in the local area around the caldera, as well as the Ikedako ashfall, which is relatively widespread in this region but of only 2.5 km^3 volume (Inakura et al., 2014) and show the different geochemical trends in whole rock composition of the 6.9 ka eruption (Kawanabe and Sakagachi, 2005). Thus, the 7.3 ka K-Ah eruption is the only source of the widely distributed uppermost unit S-1 that overlies the depositional sequence of the last glacial period. These stratigraphic interpretations of unit S-1 and St were confirmed by core samples obtained from drilling sites 4 km north of Takeshima Island during Drilling

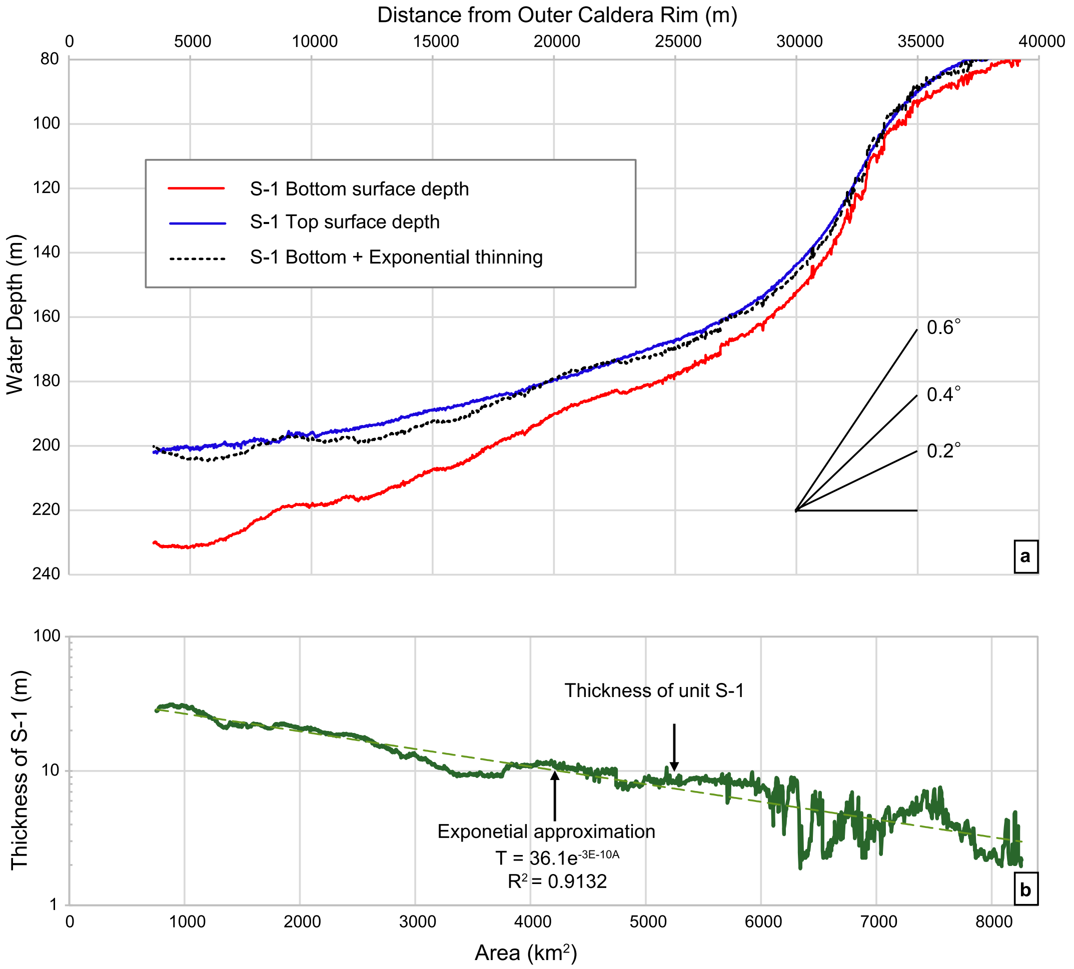

Fig. 6. Geomorphology of unit S-1.
(a) Morphology of the top and bottom surfaces of unit S-1 along the seismic line 3; reference dotted line representing the approximate exponential thickness decay with increasing distance added on the bottom depth. (b) Logarithmic thickness of unit S-1 against the area and the exponential approximation using eq. (3) is shown by the dashed line.

Vessel Chikyu Expedition 912 (Tatsumi et al., 2020). The chemical composition indicates that the entire unit S-1 up to the lower boundary is a K-Ah eruption product, and the age and chemical composition analysis indicate that the volcanic unit St is pre-K-Ah (Nakaoka et al., 2022; Hanyu et al., 2022).

5.2. *Possible emplacement mechanism of unit S-1*

The submarine distribution, morphology, and prominent facies of unit S-1 originating from the K-Ah eruption provide information on its emplacement mechanism, including secondary mass transport. Unit S-1 on the east side of the caldera is likely well preserved as a *syn*-eruptive deposition, and there is no evidence of secondary mass movement, at least in the seismic resolution. An extensive caldera rim did not develop, and a flat to very slight upslope (i.e., 0.2°) extended toward the western slope of the Tanegashima Island (Fig. 3d and e). Unit S-1 traverses a gentle slope (i.e., 0.7°) over the shelf break southwest of the Tanegashima Island (Fig. 3e) and abruptly terminates before the shelf break on a steep slope (i.e., 2.9°) west of the Tanegashima Island (Fig. 3d). Thus, unit S-1 on the east side of the caldera should represent syn-eruptive deposition. Conversely, deformation structures that could have been caused by gravitational instability are evident (Fig. 4): slumping from the northern to the western part of the caldera slope, debris flow resting on the center of the basin floor (Fig. 3a), and debris avalanches deposits with a hummocky topography at the southwestern high to the flank of the caldera rim. For example, the chaotic facies around the deepest part of the basin floor are typical seismic facies of a debris flow (e.g., Moscardelli and Wood, 2008), and a headwall is recognized on the eastern side of the adjacent slope (Fig. 3a). This chaotic facies also contains large blocks exhibiting the original facies of unit S-1, suggesting that this wasting took place after unit S-1 was consolidated to preserve the initial emplacement structures in the debris flow deposits. Notably, the underlying units were not significantly affected, as the base of the failures is almost identical to the lower boundary of unit S-1, and shows minor disturbances above the upper thin beds of the underlying units, most likely caused only in unit S-1.

Unit S-1 on the east side of the caldera exhibits thinning with increasing distance from the caldera; the thinning is approximately exponential, thereby providing insight into how the unit was emplaced. Fig. 6a depicts the boundaries of the upper and bottom surfaces of unit S-1 profiled from the caldera margin to the shelf margin of the Tanegashima Island along line 3, where a nearly flat to slightly upslope seafloor forms without any seismic evidence of secondary mass movement. Seismic data provide continuous geomorphology. The continuous thinning along the distance can be approximated by Eq. (1):

$$T = T_c exp(-k_1 d) \tag{1}$$

where T is the unit thickness in meters, T_c is the thickness at the caldera margin in this case, d is the distance from there, and k_1 represents the thinning rate along the distance. The approximated exponential decay of

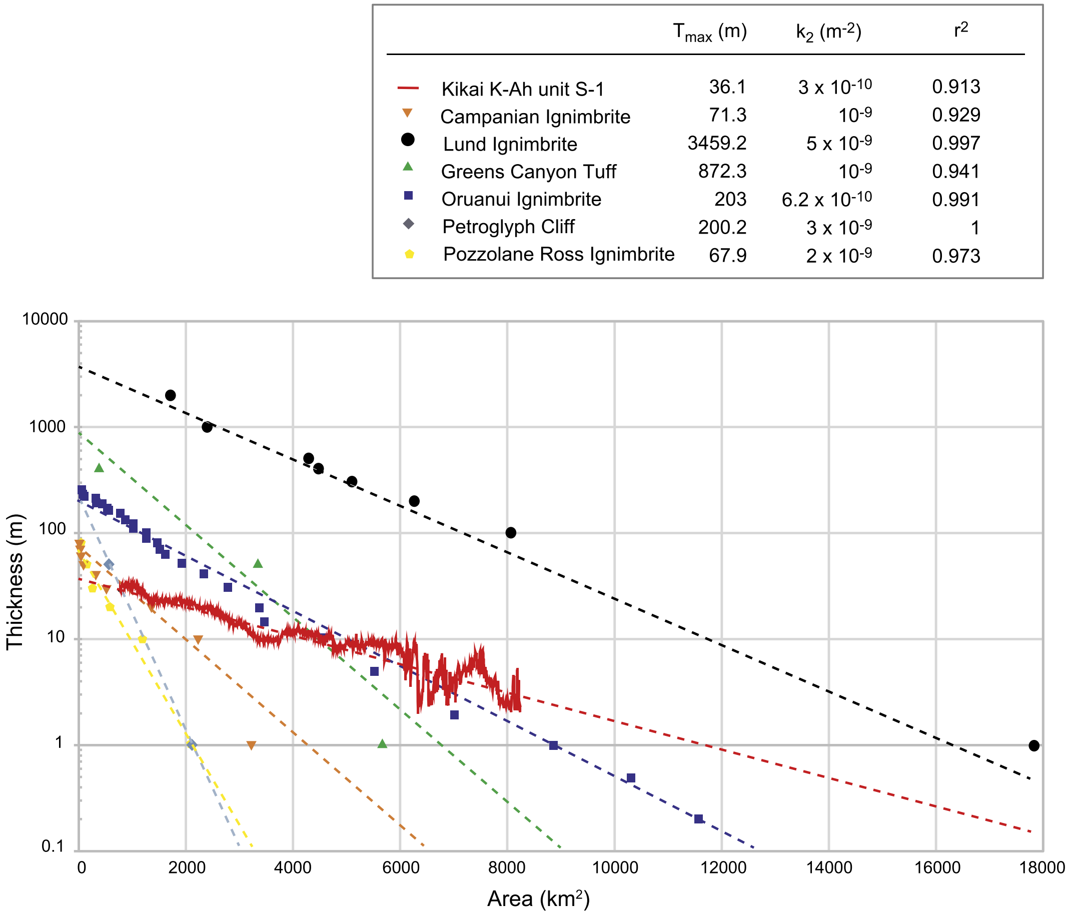

	T_{max} (m)	k_2 (m^{-2})	r^2
━ Kikai K-Ah unit S-1	36.1	3×10^{-10}	0.913
▼ Campanian Ignimbrite	71.3	10^{-9}	0.929
● Lund Ignimbrite	3459.2	5×10^{-9}	0.997
▲ Greens Canyon Tuff	872.3	10^{-9}	0.941
■ Oruanui Ignimbrite	203	6.2×10^{-10}	0.991
◆ Petroglyph Cliff	200.2	3×10^{-9}	1
⬟ Pozzolane Ross Ignimbrite	67.9	2×10^{-9}	0.973

Fig. 7. Comparison of our exponential approximation result shown in Fig. 6b with the on-land PDC deposits shown by Silleni et al. (2020).

the thickness of unit S-1 can be determined using least-square fitting:

$$T = 44.2exp\left(-6 \times 10^{-5}d\right), \left(r^2 = 0.905\right) \tag{2}$$

where r^2 is the coefficient of determination by least squares. Another expression between the unit thickness and the cumulative area from the center of the caldera, A, which was used for on-land ignimbrite by Wilson (1991), is presented as Eq. (3):

$$T = T_{max}exp(-k_2A) \tag{3}$$

where T_{max} is the maximum thickness, and k_2 represents the relationship between the unit thickness and the cumulative area. Subsequently, unit S-1 is approximated as Eq. (4) and shown in Fig. 6b:

$$T = 36.1exp\left(-3 \times 10^{-10}A\right), \left(r^2 = 0.913\right) \tag{4}$$

Unit S-1 fills pre-existing local topographic lows. The deviation from the exponential decay curve can be reflected by pre-existing topographic effects on the deposition of the unit. This is evident in Fig. 6a, where unit S-1 creates a smooth seafloor surface exhibiting a positive deviation from the curve obtained by appending the exponential decay thickness of Eq. (2) to the bottom surface of the unit (i.e., pre-existing seafloor for the deposition of unit S-1). Hence, unit S-1 tends to fill pre-existing basins, depressions, and fault-related displacements, forming a smooth submarine topography.

The exponential thinning and depression-filling nature of the submarine pyroclastic unit S-1 suggests that it predominantly originates from the emplacement of density current. The characteristic exponential decay is commonly observed in PDC deposits (Wilson, 1991; Silleni et al., 2020), and is also reproduced by subaerial/subaqueous laboratory experiments and theoretical modeling (Woods et al., 1998; Freundt, 2003). Furthermore, the depression-filling nature of the deposition is a typical feature of PDC (i.e., valley-ponded ignimbrite), which forms the top surface of a planer and is evident on low-aspect-ratio ignimbrites (e.g., Wilson and Walker, 1985). Our geomorphological features were similar to those of such ignimbrites. An alternative interpretation for the submarine pyroclastic unit S-1 is that it originated from the fallout deposition by sediment plumes through the water column; however, this interpretation cannot explain these depositional features. The fallout deposition demonstrated experimentally (Mcleod et al., 1999; Freundt, 2003) produces massive deposits in the proximal area and thins rapidly away from the shore. These regimes might have partially developed around the entrance of the flow into the sea. In our case, it may correspond to the transparent facies observed around the Satsuma Iwojima Island. We hypothesize that fallout deposition cannot form depression-filling features, but is rather independent of topography. Some amount of fallout should be brought from the subaerial counterpart, but it cannot explain the large volume of unit S-1; it can be incorporated into the density current as the analog experiment demonstrated (Freundt, 2003). These lines of evidence suggest that unit S-1 results from the sedimentation of the density current originating from the PDC that entered into the water. We treat unit S-1 as a depositional unit likely formed by a sustained current of the climactic phase of the eruption, the majority of which is likely the single subunit event that reached the distal island over the sea, as indicated by the subaerial deposits.

Our results suggest that the behavior of pyroclastic material after transformation into water-supported density currents is similar to that of non-volcanic dilute density currents. The dynamics and morphological characteristics of turbidites have been well studied by observations, experiments, and models (e.g., Gladstone et al., 1998; Salaheldin et al., 2000; Talling et al., 2007; Malgesini et al., 2015). Different depositional shapes, gradual thinning along the distance from the source in an exponential fashion, and lenticular shapes with broad maximum thickness at intermediate distances are observed, which are influenced by topographic effects such as lateral constraints and slope angle, volume, and physical properties of particles in the current. While there have been several studies on the morphology of turbidites, Malgesini et al. (2015) have shown that the shape of each unit is close to exponential thinning when the current has a low sediment concentration (<10% by volume), which does not intensify the hindered settling due to particle interactions, otherwise a broad maximum thickness is formed far from the source, which is observed in most other mass transport deposits. Turbidites are also known to bury geomorphic variations across a range of topographic scales (e.g., Mutti et al., 2009; Kneller et al., 2016). Our geomorphological features were also similar to such features of turbidities.

The values of k_1 and k_2 are decay constants of the exponential function in Eqs. (1) and (3), which are useful for quantitative comparisons with those for on-land ignimbrites and for non-volcanic density currents. The k_2 value for the submarine pyroclastic unit S-1 is 3×10^{-10} m^{-2} which is notably smaller that of on-land ignimbrites (Silleni et al., 2020), suggesting the effect of slower settling velocity in water is substantial. The k_2 parameter is proportional to the settlement velocity and inversely proportional to the volume flux of the eruption, as given by the theoretical expression of Woods et al. (1998). Our k_2 value of 3×10^{-10} m^{-2} was lower than those reported by Silleni et al. (2020), who showed that k_2 values range from 5×10^{-10} to 3×10^{-9} m^{-2} on historical on-land ignimbrites, including Oruanui and Lund ignimbrites from supereruptions (Fig. 7). The observed lower k_2 value of unit S-1 indicates a lower settling velocity and/or higher volume flux of the eruption. We suggest that the observed lower k_2 value is due to the slower settlement velocity in water, as we believe that the volumetric flux of eruptive material introduced into the water during the K-Ah eruption would not have exceeded that of the historical on-land ignimbrites from the supereruptions. Due to the reduced gravity in water, the settling velocity of particles in subaqueous density current can be lower by an order of magnitude than that in subaerial flow entraining hot air. Given the volume flux in water, a slower settling velocity in a subaqueous environment leads to a relatively long runout deposition.

The k_1 value for the submarine pyroclastic unit S-1 is 6×10^{-5} m^{-2}, which is similar to that of the turbidites formed by dilute density current; The k_1 values of turbidities showing exponential thinning shown by Malgesini et al. (2015) are on the order of 10^{-5} m^{-2}, suggesting that unit S-1 may have been formed by dilute water-supported density current. Furthermore, the available thickness distribution of pyroclastic deposits using vibrocore sampling (Trofimovs et al., 2008) shows a similar trend. It was emplaced by water-supported density currents transformed by PDCs from the 2003 dome collapse on the Soufriere Hills volcano, Montserrat, and the thin (< 1 m) unit extends to approximately 40 km from the source. We calculate the thinning rate of this unit using Eq. (1), which gives a k_1 value of the order of 10^{-5} m^{-2}. Our quantitative comparisons of the k_1 values, including that for non-volcanic density currents, indicate that subaerial PDCs entering into the water are transported as dilute density currents, suggesting that the pyroclastic material is well mixed with the water once it enters into the water. Furthermore, climbing slopes is a peculiar feature of a dilute density current. Unit S-1 shows that the dilute density current climbed the very gentle slope ($< 1^\circ$), terminated at the slopes of about 3°, and passed over the height of approximately 150 m (Fig. 3a, d, and e). The fact that this occurred for most of the long runout distances is remarkable. Climbing slopes have also been reported in dilute non-volcanic turbidity currents (Muck and Underwood, 1990; Talling et al., 2007) and water-supported density currents derived from PDC (Trofimovs et al., 2008).

The formation of dilute density currents derived from subaerial PDCs that enter the water may require a certain depth of water to be present. Our results are different in geomorphological features from the well-documented submarine ignimbrite of the 1883 Krakatau caldera-forming eruption occurring in shallow sea (i.e., 40 m average water depth), implying that water depth may influence the generation of density currents; the deposition of pyroclastic material supplied by PDCs at shallow water depths may be more complex. In the shallow-marine environment of the 1883 Krakatau eruption, the major deposition did not appear with systematic thinning, at least in the proximal area (at a distance of up to ~20 km from the source), but rather a mottle-like thickening distribution that did not fill pre-existing depressions but rather bypassed them (Sigurdsson et al., 1991; Self, 1992; Mandeville et al., 1996). The dominant depositional mode of the distal area was not the same as that of the proximal area, but the geomorphology seen in the large area around Krakatau is different from that of unit S-1. Since laboratory experiments indicate that seafloor-hugging of density currents occurs only in deep waters that exhibit exponential thinning (Freundt, 2003), the Krakatau eruption could be a case where the water depth is not deep enough to form a density current and more complex deposition occurs in the shallow marine environment, particularly in the proximal area. In contrast, the Kikai caldera is located at a depth of >200 m, which is deeper if compared to the thickness of such pyroclastic deposits; the water depth is deep enough that incoming PDC could generate a large ash-water mixing regime near the entry zone and form a dilute density current, thus creating an extensive exponentially thinning deposit. This is consistent with laboratory experiments showing that a smooth transition of bulk flow from air into water does not occur until the flow thickness is >40–60% of the water depth (Freundt, 2003). Thus, we propose that the formation of dilute density currents transformed by PDCs probably requires sufficient water depth, as inferred also from previous analog experiments (Freundt, 2003).

5.3. Eruptive volume of the Kikai-Akahoya eruption

We reconstructed the K-Ah eruption volume, where submarine deposits were estimated from our study, and on-land ignimbrite, Plinian, and co-ignimbrite air-fall deposits from earlier studies. First, we estimated, based on our isopach map, that the bulk volume of the submarine deposits of the K-Ah eruption, which predominantly originated from the PDC, is 71 km^3. We include the volume of secondary mass movements in the volume calculation because these mostly occurred in unit S-1 and involved very small parts of the underlying layer. This estimate is likely conservative as the present seismic resolution limits the extension of unit S-1 to ~3 m thickness at the distal margin when in reality the thinning of the unit continues further inside and outside the survey area. Nevertheless, even this conservative estimate of 71 km^3, is much larger than the previous estimate (i.e., 30–45 km^3; Maeno and Taniguchi, 2007). The volume of the Koya (i.e., on-land) ignimbrite, which traveled over the sea and was placed in the distal islands, was estimated to be 5 km^3 by simply assuming an average thickness of 1 m in the distribution area reported by Ui (1973). The total bulk volume of the subaerial and subaqueous ignimbrites of the K-Ah eruption was 76 km^3. The volume of the air-fall ash emplaced on the Koya ignimbrite was more significant. The widespread tephra, i.e., the Akahoya ash deposit, is the most notable and well-studied Holocene time-marking tephra in Japan (Machida and Arai, 1978, 2003; Chen et al., 2022; Smith et al., 2013). In addition to rigorous field studies at locations across the Japanese archipelago (e.g., Machida and Arai, 1978), submarine sediment cores have sampled these deposits around Japan (e.g., Furuta et al., 1986). An isopach map was compiled from subaerial and submarine samples covering an extensive area (Machida and Arai, 2003), and Suto et al. (2007) updated this volume calculation to 374 km^3 from the mesh data of the isopach map of Machida and Arai (2003). This volume can be conservatively estimated

Table 1
List of major eruptions during the Holocene.

	Country	Age	Bulk volume (km^3)	DRE volume (km^3)	Mass (kg)	Source
Kikai K-Ah	Japan	7.3 ka	457	183	4.6×10^{14}	This study
Kurie Lake	Russia	6.4 ka	170	80	2.0×10^{14}	Ponomareva et al. (2004)
Mazama (Crater Lake)	United States	5.7 ka	176	61	1.5×10^{14}	Buckland et al. (2020)
Samalas	Indonesia	1257 CE		40	1.0×10^{14}	Lavigne et al. (2013)
Santorini (Minoan)	Greece	1.6 ka		35	8.6×10^{13}	Karstens et al. (2023)
Tambora	Indonesia	1815 CE	113	33	8.2×10^{13}	Self et al. (2004)

Mass is calculated from 2490 kg/m^3 for DRE.

to be 249 km^3 by omitting a large, interpolated section of the eastern area of the isopach map. The total bulk volume of the K-Ah eruption is 332–457 km^3 (133–183 km^3 in DRE, assuming deposit-density 1.0 g/cm^3), with the 7 km^3 volume of the Plinian fallout (Suto et al., 2007) serving as a precursor to the caldera-forming eruption. The K-Ah eruption, with a bulk volume of 332–457 km^3, is probably the largest Holocene eruption compared to major Holocene eruptions (Table 1).

6. Conclusion

High-resolution seismic reflection surveys, together with chemical analyses of glass shards, suggested that the structural, stratigraphic, and compositional characteristics of the uppermost unit covering an area > 4500 km^2 around the Kikai caldera consists of pyroclastic deposits of the 7.3 ka Kikai-Akahoya (K-Ah) eruption. This unit formed predominantly by density current derived from the PDC entered into the sea, exhibiting exponential thinning and depression-filling depositional features. The quantitative comparisons of geometric shape and its thinning rate, including that for non-volcanic density currents, indicate that subaerial PDC entering the water was transported as a dilute density current. We propose that the formation of dilute density currents transformed by PDCs probably requires sufficient water depth, as inferred also from previous analog experiments. The volume of the submarine deposits is estimated to be >71 km^3, comprising a total of >76 km^3 of PDC deposits with subaerial ignimbrite. The total bulk volume of the K-Ah eruption is 332–457 km^3 (133–183 km^3 in DRE), which is probably the largest Holocene eruption in the world.

Funding

This study was supported by the Ministry of Education, Culture, Sports, Science and Technology (MEXT) of Japan, under its The Second Earthquake and Volcano Hazards Observation and Research Program (Earthquake and Volcano Hazard Reduction Research) and JSPS Grant-in-Aid (20H00199).

CRediT authorship contribution statement

Satoshi Shimizu: Formal analysis, Investigation, Methodology, Visualization, Writing – original draft. **Reina Nakaoka:** Formal analysis, Investigation, Methodology, Writing – review & editing. **Nobukazu Seama:** Conceptualization, Formal analysis, Investigation, Writing – review & editing, Funding acquisition, Supervision. **Keiko Suzuki-Kamata:** Formal analysis, Investigation, Writing – review & editing. **Katsuya Kaneko:** Investigation, Writing – review & editing. **Koji Kiyosugi:** Investigation. **Hikaru Iwamaru:** Investigation. **Mamoru Sano:** Investigation. **Tetsuo Matsuno:** Investigation, Writing – review & editing. **Hiroko Sugioka:** Project administration. **Yoshiyuki Tatsumi:** Conceptualization, Supervision, Writing – review & editing.

Declaration of competing interest

The authors declare the following financial interests/personal relationships which may be considered as potential competing interests:

Nobukazu Seama reports financial support was provided by Ministry of Education, Culture, Sports, Science and Technology (MEXT) of Japan. Nobukazu Seama reports financial support was provided by Japan Society for the Promotion of Science (JSPS).

Data availability

Data will be made available on request.

Acknowledgments

We acknowledge the crews and all research members who participated in the cruises of T/S Fukae Maru and R/V Shinsei Maru KS-19-17 for their contribution to the data and sample acquisition. We also thank the staff of KOBEC (ocean-bottom exploration center Kobe University) for their continuous support. Finally, special thanks are due to two anonymous reviewers for their thoughtful reviews and many insightful and careful comments that improved our draft, and to J. L. Macias for his efforts in the editing of this paper.

Appendix A. Supplementary data

Supplementary data to this article can be found online at https://doi.org/10.1016/j.jvolgeores.2024.108017.

References

Allen, S.R., Cas, R.A.F., 2001. Transport of pyroclastic flows across the sea during the explosive rhyolitic eruption of the Kos Plateau Tuff, Greece. Bull. Volcanol. 62 (6–7), 441–456. https://doi.org/10.1007/s004450000107.

Allen, S.R., Freundt, A., Kurokawa, K., 2012. Characteristics of submarine pumice-rich density current deposits sourced from turbulent mixing of subaerial pyroclastic flows at the shoreline : field and experimental assessment. Bull. Volcanol. 74, 657–675. https://doi.org/10.1007/s00445-011-0553-1.

Buckland, H.M., Cashman, K.V., Engwell, S.L., Alison, C.R., 2020. Sources of uncertainty in the Mazama isopachs and the implications for interpreting distal tephra deposits from large magnitude eruptions. Bull. Volcanol. 82, 23. https://doi.org/10.1007/s00445-020-1362-1.

Bursik, M.I., Woods, A.W., 1996. The dynamics and thermodynamics of large ash flows. Bull. Volcanol. 58, 175–193. https://doi.org/10.1007/s004450050134.

Carey, S.N., Sigurdsson, H., 1980. The Roseau ash: Deep-sea tephra deposits from a major eruption on Dominica, lesser antilles arc. J. Volcanol. Geotherm. Res. 7 (1–2), 67–86. https://doi.org/10.1016/0377-0273(80)90020-7.

Carey, S., Sigurdsson, H., Mandeville, C., Bronto, S., 1996. Pyroclastic flows and surges over water: an example from the 1883 Krakatau eruption. Bull. Volcanol. 57 (7), 493–511. https://doi.org/10.1007/BF00304435.

Cas, R.A., Wright, J.V., 1991. Subaqueous pyroclastic flows and ignimbrites: an assessment. Bull. Volcanol. 53, 357–380. https://doi.org/10.1007/BF00280227.

Cas, R.A.F., Wright, H.M.N., Folkes, C.B., Lesti, C., Porreca, M., Giordano, G., Viramonte, J.G., 2011. The flow dynamics of an extremely large volume pyroclastic flow, the 2.08-Ma Cerro Galán Ignimbrite, NW Argentina, and comparison with other flow types. Bull. Volcanol. 73, 1583–1609. https://doi.org/10.1007/s00445-011-0564-y.

Chen, X.Y., Blockley, S.P.E., Fletcher, R., Zhang, S., Kim, J.H., Park, M.H., Chen, C., Yin, J., Xu, Y.G., 2022. Holocene Tephrostratigraphy in the East Sea/Japan Sea: Implications for Eruptive history of Ulleungdo Volcano and potential for Hemispheric Synchronization of Sedimentary Archives. J. Geophys. Res. Solid Earth 127 (2). https://doi.org/10.1029/2021JB023243.

Cole, P.D., Calder, E.S., Druitt, T.H., Hoblitt, R., Robertson, R., Sparks, R.S.J., Young, S. R., 1998. Pyroclastic flows generated by gravitational instability of the 1996-97 lava dome of Soufriere Hills Volcano, Montserrat. Geophys. Res. Lett. 25 (18), 3425–3428. https://doi.org/10.1029/98GL01510.

Dade, W.B., Huppert, H.E., 1996. Emplacement of the Taupo ignimbrite by a dilute turbulent flow. Nature 381, 509–512. https://doi.org/10.1038/381509a0.

Fisher, R.V., Orsi, G., Ort, M., Heiken, G., 1993. Mobility of a large-volume pyroclastic flow - emplacement of the Campanian ignimbrite, Italy. J. Volcanol. Geotherm. Res. 56 (3), 205–220. https://doi.org/10.1016/0377-0273(93)90017-L.

Freundt, A., 2003. Entrance of hot pyroclastic flows into the sea: Experimental observations. Bull. Volcanol. 65, 144–164. https://doi.org/10.1007/s00445-002-0250-1.

Freundt, A., Schindlbeck-Belo, J.C., Kutterolf, S., Hopkins, J.L., 2022. Tephra layers in the marine environment: a review of properties and emplacement processes. Geol. Soc. Spec. Publ. 520 https://doi.org/10.1144/SP520-2021-50.

Fujihara, M., Suzuki-Kamata, K., 2013. Glass composition and emplacement mode of Koya Pyroclastic flow deposit and its proximal equivalent. Bull. Volcanol. Soc. Jpn. 58, 489–498 (in Japanese with English abstract). 10.18940/kazan.58.4_489.

Furuta, T., Fujioka, K., Arai, F., 1986. Widespread submarine tephras around Japan–Petrographic and chemical properties. Mar. Geol. 72, 125–142. https://doi.org/10.1016/0025-3227(86)90103-9.

Geshi, N., Maeno, F., Nakagawa, S., Naruo, H., Kobayashi, T., 2017. Tsunami deposits associated with the 7.3 ka caldera-forming eruption of the Kikai Caldera, insights for tsunami generation during submarine caldera-forming eruptions. J. Volcanol. Geotherm. Res. 347, 221–233. https://doi.org/10.1016/j.jvolgeores.2017.09.015.

Gladstone, C., Phillips, J.C., Sparks, R.S.J., 1998. Experiments on bidisperse, constant-volume gravity currents: Propagation and sediment deposition. Sedimentology 45 (5), 833–843. https://doi.org/10.1046/j.1365-3091.1998.00189.x.

Hanyu, T., Chang, Q., Kaneko, K., Nakaoka, R., Kiyosugi, K., Suzuki-Kamata, K., Yamamoto, Y., Matsuno, T., Seama, N., Tatsumi, Y., 2022. Chemical evolution of magma toward the catastrophic eruption at Kikai Caldera recorded in Chikyu SCORE tephra. In: Annual Meeting of GSJ 2022.

Hart, K., Carey, S., Sigurdsson, H., Sparks, R.S.J., Robertson, R.E.A., 2004. Discharge of pyroclastic flows into the sea during the 1996-1998 eruptions of the Soufrière Hills volcano, Montserrat. Bull. Volcanol. 66 (7), 599–614. https://doi.org/10.1007/s00445-004-0342-1.

Inakura, H., Naruo, H., Okuno, M., Kobayashi, T., 2014. Eruptive history of Ikeda Volcano, Ibusuki Area, Southern Kyushu, Japan. Kazan 59, 255–268 (in Japanese with English abstract). 10.18940/kazan.59.4_255.

Jutzeler, M., Manga, M., White, J.D.L., Talling, P.J., Proussevitch, A.A., Watt, S.F.L., Cassidy, M., Taylor, R.N., le Friant, A., Ishizuka, O., 2017. Submarine deposits from pumiceous pyroclastic density currents traveling over water: an outstanding example from offshore Montserrat (IODP 340). Geol. Soc. Am. Bull. 129 (3–4), 392–414. https://doi.org/10.1130/B31448.1.

Karstens, J., Crutchley, G.J., Berndt, C., Talling, P.J., Watt, S.F.L., Hühnerbach, V., Le Friant, A., Lebas, E., Trofimovs, J., 2013. Emplacement of pyroclastic deposits offshore Montserrat: Insights from 3D seismic data. J. Volcanol. Geotherm. Res. 257, 1–11. https://doi.org/10.1016/j.jvolgeores.2013.03.004.

Karstens, J., Preine, J., Crutchley, G.J., Kutterolf, S., van der Bilt, W.G.M., Hooft, E.E.E., Druitt, T.H., Schmid, F., Cederstrøm, J.M., Hübscher, C., Nomikou, P., Carey, S., Kühn, M., Elger, J., Berndt, C., 2023. Revised Minoan eruption volume as benchmark for large volcanic eruptions. Nat. Commun. 14 (1) https://doi.org/10.1038/s41467-023-38176-3.

Kawanabe, Y., Sakagachi, K., 2005. Geology of the Kaimon Dake district. In: Quadrangle Series, 1:50,000, Geol. Surv. Japan. AIST, 82 p. (in Japanese with English abstract 3 p).

Kneller, B., Dykstra, M., Fairweather, L., Milana, J.P., 2016. Mass-transport and slope accommodation: Implications for turbidite sandstone reservoirs. Am. Assoc. Pet. Geol. Bull. 100 (2), 213–235. https://doi.org/10.1306/09011514210.

Lavigne, F., Degeai, J.P., Komorowski, J.C., Guillet, S., Robert, V., Lahitte, P., Oppenheimer, C., Stoffel, M., Vidal, C.M., Suronoh Pratomo, I., Wassmer, P., Hajdas, I., Hadmoko, D.S., de Belizal, E., 2013. Source of the great A.D. 1257 mystery eruption unveiled, Samalas volcano, Rinjani Volcanic complex, Indonesia. Proc. Natl. Acad. Sci. U. S. A. 110 (42), 16742–16747. https://doi.org/10.1073/pnas.1307520110.

Legros, F., Druitt, T.H., 2000. On the emplacement of ignimbrite in shallow-marine environments. J. Volcanol. Geotherm. Res. 95 (1–4), 9–22. https://doi.org/10.1016/S0377-0273(99)00116-X.

Machida, H., 1999. The stratigraphy, chronology and distribution of distal marker-tephras in and around Japan. Glob. Planet. Chang. 21 (1–3), 71–94. https://doi.org/10.1016/S0921-8181(99)00008-9.

Machida, H., Arai, F., 1978. Akahoya Ash-A holocene widespread tephra erupted from the Kikai Caldera, South Kyushu, Japan. Quat. Res. 17, 143–163. https://doi.org/10.4116/jaqua.17.143.

Machida, H., Arai, F., 2003. Atlas of Tephra in and around Japan. Unive of Tokyo Press, p. 336 (in Japanese).

Maeno, F., Taniguchi, H., 2007. Spatiotemporal evolution of a marine caldera-forming eruption, generating a low-aspect ratio pyroclastic flow, 7.3 ka, Kikai caldera, Japan: Implication from near-vent eruptive deposits. J. Volcanol. Geotherm. Res. 167, 212–238. https://doi.org/10.1016/j.jvolgeores.2007.05.003.

Malgesini, G., Talling, P.J., Hogg, A.J., Armitage, D., Goater, A., Felletti, F., 2015. Quantitative analysis of submarine-flow deposit shape in the Marnoso-Arenacea formation: what is the signature of hindered settling from dense near-bed layers? J. Sediment. Res. 85 (2), 170–191. https://doi.org/10.2110/jsr.2015.15.

Mandeville, C.W., Carey, S., Sigurdsson, H., 1996. Sedimentology of the Krakatau 1883 submarine pyroclastic deposits. Bull. Volcanol. 57, 512–529. https://doi.org/10.1007/BF00304436.

McLeod, P., Carey, S., Stephen, J., Sparks, R., 1999. Behaviour of particle-laden flows into the ocean: Experimental simulation and geological implications. Sedimentology 46, 523–536. https://doi.org/10.1046/j.1365-3091.1999.00229.x.

Moscardelli, L., Wood, L., 2008. New classification system for mass transport complexes in offshore Trinidad. Basin Res. 20 (1), 73–98. https://doi.org/10.1111/j.1365-2117.2007.00340.x.

Muck, M.T., Underwood, M.B., 1990. Upslope flow of turbidity currents: a comparison among field observations, theory, and laboratory models. Geology 18 (1), 54–57. https://doi.org/10.1130/0091-7613(1990)018<0054:UFOTCA>2.3.CO;2.

Mutti, E., Bernoulli, D., Lucchi, F.R., Tinterri, R., 2009. Turbidites and turbidity currents from alpine "flysch" to the exploration of continental margins. Sedimentology 56 (1), 267–318. https://doi.org/10.1111/j.1365-3091.2008.01019.x.

Nakaoka, R., Kaneko, K., Seama, N., Suzuki-Kamata, K., Kiyosugi, K., Hanyu, T., Yamamoto, Y., Matsuno, T., Shimizu, S., Sugioka, H., Tatsumi, T., 2022. Characteristics of Kikai Caldera volcanic products revealed by seafloor core samples. In: Annual Meeting of GSJ 2022.

Ono, K., Soya, T., Hosono, T., 1982. Geology of the Satsuma-Io-Jima District. quadrangle series, scale 1:50000. Geol. Surv. Jpn. 1–80.

Park, J.-O., Kimura, M., Taira, A., 1996. Late Pleistocene unconformity of the Tsushima and Korea Straits revealed by seismic reflection profiles. J. Geogr. 105, 297–305. https://doi.org/10.5026/JGEOGRAPHY.105.3_297.

Ponomareva, V.V., Kyle, P.R., Melekestsev, I.V., Rinkleff, P.G., 2004. The 7600 (14 C) year BP Kurile Lake caldera-forming eruption, Kamchatka, Russia: stratigraphy and field relationships. J. Volcanol. Geotherm. Res. 136, 199–222. https://doi.org/10.1016/j.jvolgeores.2004.05.013.

Robinson, N., Regetz, J., Guralnick, R.P., 2014. EarthEnv-DEM90: a nearly-global, void-free, multi-scale smoothed, 90m digital elevation model from fused ASTER and SRTM data. ISPRS J. Photogramm. 87, 57–67. https://doi.org/10.1016/j.isprsjprs.2013.11.002.

Roche, O., Buesch, D.C., Valentine, G.A., 2016. Slow-moving and far-travelled dense pyroclastic flows during the Peach Spring super-eruption. Nat. Commun. 7, 1–8. https://doi.org/10.1038/ncomms10890.

Saito, Y., 1998. Sea levels of the last glacial in the East China Sea continental shelf. Quat. Res. 37, 235–242 (in Japanese with English abstract). https://doi.org/10.4116/jaqua.37.235.

Saito, G., Kazahaya, K., Shinohara, H., Stimac, J., Kawanabe, Y., 2001. Variation of volatile concentration in a magma system of Satsuma-Iwojima volcano deduced from melt inclusion analyses. J. Volcanol. Geotherm. Res. 108, 11–31. https://doi.org/10.1016/S0377-0273(00)00276-6.

Salaheldin, T.M., Imran, J., Chaudhry, M.H., Reed, C., 2000. Role of fine-grained sediment in turbidity current flow dynamics and resulting deposits. Mar. Geol. 171 (1–4), 21–38. https://doi.org/10.1016/S0025-3227(00)00114-6.

Self, S., 1992. Krakatau revisited: the course of events and interpretation of the 1883 eruption. GeoJournal 28 (2), 109–121. https://doi.org/10.1007/BF00177223.

Self, S., Gertisser, R., Thordarson, T., Rampino, M.R., Wolff, J.A., 2004. Magma volume, volatile emissions, and stratospheric aerosols from the 1815 eruption of Tambora. Geophys. Res. Lett. 31 (20), 10–13. https://doi.org/10.1029/2004GL020925.

Sigurdsson, H., Carey, S., Mandeville, C., Bronto, S., 1991. Pyroclastic flows of the 1883 Krakatau eruption. Eos 72, 377–381. https://doi.org/10.1029/90EO00286.

Sigurdsson, H., Carey, S., Alexandri, M., Vougioukalakis, G., Croff, K., Roman, C., Sakellariou, D., Anagnostou, C., Rousakis, G., Ioakim, C., Gogou, A., Ballas, D., Misaridis, T., Nomikou, P., 2006. Marine investigations of Greece's Santorini volcanic field. Eos 87 (34), 337–342. https://doi.org/10.1029/2006EO340001.

Silleni, A., Giordano, G., Isaia, R., Ort, M.H., 2020. The magnitude of the 39.8 ka campanian ignimbrite eruption, Italy: method, uncertainties and errors. Front. Earth Sci. 8, 1–22. https://doi.org/10.3389/feart.2020.543399.

Smith, V.C., Staff, R. A, Blockley, S.P.E., Bronk Ramsey, C., Nakagawa, T., Mark, D.F., Takemura, K., Danhara, T., 2013. Identification and correlation of visible tephras in the Lake Suigetsu SG06 sedimentary archive, Japan: Chronostratigraphic markers for synchronising of east Asian/West Pacific palaeoclimatic records across the last 150 ka. In. Quat. Sci. Rev. 67, 121–137. https://doi.org/10.1016/j.quascirev.2013.01.026.

Sparks, R.S.J., Huang, T.C., 1980. Geol. Mag. 117 (5), 425–436. https://doi.org/10.1017/S0016756800028533.

Suter, J.R., Berryhill, H.L., Penland, S., 1987. Late Quaternary Sea-level fluctuations and depositional sequences, Southwest Louisiana continental shelf. Sea-level Fluct. Coast. Evol. 199–219 https://doi.org/10.2110/pec.87.41.0199.

Suto, S., Inomata, T., Sasaki, H., Mukoyama, S., 2007. Data base of the volcanic ash fall distribution map of Japan. Bull. Geol. Surv. Jpn. 58 (9/10), 261–321 (in Japanese with English abstract). https://doi.org/10.9795/bullgsj.58.261.

Talling, P.J., Amy, L.A., Wynn, R.B., 2007. New insight into the evolution of large-volume turbidity currents: Comparison of turbidite shape and previous modelling results. Sedimentology 54 (4), 737–769. https://doi.org/10.1111/j.1365-3091.2007.00858.x.

Tatsumi, Y., Suzuki-Kamata, K., Matsuno, T., Ichihara, H., Seama, N., Kiyosugi, K., Nakaoka, R., Nakahigashi, K., Takizawa, H., Hayashi, K., Chiba, T., Shimizu, S., Sano, M., Iwamaru, H., Morozumi, H., Sugioka, H., Yamamoto, Y., 2018. Giant rhyolite lava dome formation after 7.3 ka supereruption at Kikai caldera, SW Japan. Sci. Rep. 8, 1–9. https://doi.org/10.1038/s41598-018-21066-.

Tatsumi, Y., Kaneko, K., Okutsu, N., Aoile, K., 2020. The Exp.912-Leg.2 Shipboard Scientists, 2020. JAMSTEC Chikyu SCORE Expedition 912 Leg 2 Preliminary Cruise Report. https://doi.org/10.17596/0003799.

Trofimovs, J., Sparks, R.S.J., Talling, P.J., 2008. Anatomy of a submarine pyroclastic flow and associated turbidity current: July 2003 dome collapse, Soufrière Hills volcano, Montserrat, West Indies. Sedimentology 55, 617–634. https://doi.org/10.1111/j.1365-3091.2007.00914.x.

Trofimovs, J., Foster, C., Sparks, R.S.J., Loughlin, S., le Friant, A., Deplus, C., Porritt, L., Christopher, T., Luckett, R., Talling, P.J., Palmer, M.R., le Bas, T., 2012. Submarine pyroclastic deposits formed during the 20th May 2006 dome collapse of the

Soufrière Hills Volcano, Montserrat. Bull. Volcanol. 74 (2), 391–405. https://doi.org/10.1007/s00445-011-0533-5.

Ui, T., 1973. Exceptionally far-reaching, thin pyroclastic flow in Southern Kyushu. Japan. Bull. Volcanol. Soc. Jpn. 18, 153–168 (in Japanese with English abstract). 10.18940/kazanc.18.3_1.

Walker, G.P.L., McBroome, L.A., Caress, M.E., 1984. Products of the Koya Eruption from the Kikai Caldera, Japan. A Progress Report of the U.S.–Japan Cooperative Science Program, pp. 4–8.

Wilson, C.J.N., 1991. Ignimbrite morphology and the effects of erosion: a New Zealand case study. Bull. Volcanol. 53, 635–644. https://doi.org/10.1007/BF00493690.

Wilson, C.J.N., Walker, G.P.L., 1985. The Taupo eruption. New Zealand: I. General aspects. Philos. Trans. R. Soc. Lond. A314, 199–228. https://doi.org/10.1098/rsta.1985.0019.

Woods, A.W., Bursik, M.I., Kurbatov, A., v., 1998. The interaction of ash flows with ridges. Bull. Volcanol. 60 (1), 38–51. https://doi.org/10.1007/s004450050215.

Yamamoto, T., 2015. Cumulative volume step-diagrams for eruptive magmas from major Quaternary volcanoes in Japan. In: GSJ Open-File Rep. 613, Geological Survey of Japan. AIST. https://www.gsj.jp/researches/openfile/openfile2014/openfile0613.html.

Yoo, D.G., Park, S.C., 1997. Late Quaternary lowstand wedges on the shelf margin and trough region of the Korea Strait. Sediment. Geol. 109, 121–133. https://doi.org/10.1016/S0037-0738(96)00035-8.